ORIGINAL PAPER

CrossMark

Self-catalyzed surface grafting of Mn_3O_4 nanoparticles with polylactide and its magnetic properties

Anuradha Rathore[1] · Harjinder Kaur[1] · Rafael Luque[2]

Abstract Magnetic properties of nanoparticles are size dependent and surface grafting of nanoparticles not only prevents their agglomeration but can also lead to effective domains separation. Present study deals with the synthesis of manganese oxide nanoparticles (< 5 nm) by microwave assisted solvothermal process and its grafting with poly L-lactic acid by a self-catalyzed ring opening polymerization of L-lactide. The Mn_3O_4 nanoparticles and Mn_3O_4/PLLA nanocomposite were characterized by many analytical techniques such as FT-IR, TEM, ^{1}H NMR, ^{13}C NMR, XRD, XPS, TGA and DSC etc. The magnetic properties of nanoparticles and nanocomposites were studied using VSM and SQUID showed marked shift in magnetic behavior of Mn_3O_4 nanoparticles which were super paramagnetic, on coating with PLLA.

Introduction

In the past few years efforts have been made to develop and characterize nanomaterials having unique properties (optical, electrical or magnetic). Due to such properties these nanomaterials have found applications in the field of electronics, optics, aerospace, medicine, fuel cells etc. [1, 2]. Especially noteworthy is their contribution in the field of biomedicine and biotechnology as nanoparticles can interact with biological systems at the molecular level [3, 4]. Among the variety of nanomaterials investigated for biomedical applications, magnetic nanoparticles play a prominent role in the area of magnetic separation [5], biosensors [6], contrast agents for magnetic resonance imaging, [7–9], drug delivery [10–12] tissue repair [13], hyperthermia [14, 15] storage of information [16] color imaging [17], and magnetic refrigeration [18] etc. Therefore synthesizing nanoparticles with magnetic

✉ Harjinder Kaur
   hk_ss_in@yahoo.com

✉ Rafael Luque
   q62alsor@uco.es

[1] Department of Chemistry, School of Sciences, Gujarat University, Ahmedabad, India

[2] Departamento de Quimica Organica, Universidad de Cordoba, Edif. Marie Curie, CtraNnal IV, 14014 Cordoba, Spain

properties is very important [19, 20]. The main features affecting the magnetic properties of materials are particle size, surface aspects and domain separation [21, 22].

Till date, iron oxide nanoparticles are the most frequently employed materials for magnetic and electrical properties [23]. Magnetic properties of oxides of manganese are comparatively less explored in spite of their low cost and low toxicity. In comparison to other electrically conductive metal oxides, manganese oxide stores electrical charge by double insertion of electrons and cations into the solid state [20]. Manganese shows many oxidation states (II –IV) and hence a large number of manganese oxides such as MnO, Mn_2O_3 and Mn_3O_4 are possible [24]. Magnetic properties of materials shows drastic change when particle size become similar to the distinctive length of magnetic interaction or length of spin diffusion implying that nanoscale material can have magnetic properties different from bulk form [21, 22]. The magnetic properties of manganese oxides vary from anti ferromagnetic to ferromagnetic. These properties depend on three factors oxidation state, crystal structure and the finite size [24]. The most stable among the oxides of manganese, Mn_3O_4 is a soft magnetic material and its magnetic properties at nanoscale are of great interest for researchers [25]. As the nanoparticles are prone to agglomeration due to high surface energy, their stability and hence, the magnetic properties can be enhanced by coating them with suitable agents. Polymer coating, especially by grafting onto surface of nanoparticles, can enhance their magnetic properties immensely by efficient domain separation.

In the present work we report synthesis of Mn_3O_4 nanoparticles by microwave enhanced solvothermal process and grafted them with PLLA a renewable and biodegradable polymer [26]. The effect of polylactide coating on the magnetic properties of nanocomparticles was studied. PLLA was grafted onto manganese oxide by self-catalyzed ring opening polymerization of L-lactide. Polymerization was carried out by taking various concentrations of nanoparticles and resulting composites were characterized using various analytical techniques Such as TEM, SEM, IR, NMR, TGA and DSC. At 5% Mn_3O_4/PLLA beautiful core shell structures were observed and this material was studied for its magnetic properties using VSM and SQUID.

Experimental

Material

All chemicals used were of analytical grade or of highest purity available. L-lactide was purchased from Aldrich. Manganese acetate was purchased from Qualigens fine chemicals. All the chemicals were used as received.

Synthesis of Mn_3O_4 nanoparticles

Mn_3O_4 nanoparticles were synthesized by microwave enhanced solvo thermal hydrolysis using manganese acetate and benzyl alcohol. CEM microwave operating with a power output that can be varied between 0 and 300 W was used. The solution was swiftly stirred by a magnetic stir bar to ensure homogeneity. The exposure time and temperature were programmed. In a 5 mL vessel, 1 mmol of manganese acetate and 5 mL of benzyl alcohol were placed with a magnetic bar [27]. This mixture was microwave heated at 60 °C for 3 min. Then the reaction temperature was elevated to 160 °C and kept at this temperature for 20 min. The product was collected, washed with methanol, diethyl ether and dried in oven overnight at 50 °C. Further, the nanoparticles formed were calcined in muffle furnace at 500 °C for 4 h.

PLLA grafted Mn_3O_4 nanoparticles

Different amounts of Mn_3O_4 nanoparticles were dispersed in 20 ml 1, 4-dioxane in a 50 mL round bottom flask. Reaction mixture was stirred at 60 °C using a magnetic stirrer to uniformly disperse the nanoparticles. The temperature was raised to 80 °C after the addition of 1 g of L-Lactide. The solvent was distilled off using vacuum and the temperature increased to 160 °C. After 4 h the reaction was quenched by cooling. The gelatinous mass was dispersed in chloroform, filtered and the residue washed with methanol. The product (Scheme 1) thus obtained was dried in a desiccators.

Instrumentation

Shimadzu FTIR spectrophotometer was used to analyze the synthesized compounds. Anhydrous KBr and sample were crushed using mortar pestle. Using this mixture thin pellets were made and further analysis was done.

The Transmission electron microscope (TEM) images were recorded on Hitachi (H-7500). The sample was finely powdered and dispersed in ethanol. One drop from this dispersion was kept on a 200 mesh carbon coated copper grid. After evaporating solvent, recording of images at different magnifications was done.

To study the surface morphology of synthesized nanocomposites Scanning Electron Microscope (SEM) Model JSM6100 (Jeol) with acceleration voltage range of 0.3 to 30 kV, working distance of 6–48 nm, was used.

The powder XRD of the nanoparticles was recorded on Panalytical X Pert Pro using Cu Kα radiation (= 1.54060 Å) and a filter of nickel at 40 kV and 40 mA with step size 0.03 and count time 0.7 s.

^{13}C NMR and ^{1}H NMR spectra were recorded with Bruker Avance II 400 MHz NMR spectrophotometer with $CDCl_3$ as solvent and TMS as an internal standard at room temperature.

To study thermal properties of the nanocomposites, Differential scanning calorimeter DSC-60 of Shimadzu was used.5 mg of the sample was placed on an aluminium pan, sealed and heated up to 100 °C. After cooling it to room temperature it was again scanned from ambient to 300 °C at a rate of 10 °C / min. Thermal stability of samples were determined using Thermogravimetric Analysis (TGA, Shimadzu DTG-60H). The samples were heated at the rate of 10 °C / min under nitrogen atmosphere.

XPS measurements were conducted at an ultrahigh vacuum (UHV) multipurpose surface analysis system (SpecsTM model, Germany) at the SCAI in Universidad de Cordoba (Spain), operating at pressures <10–14 MPa using a conventional X-Ray source (XR-50, Specs, Mg–K, 1253.6 eV) in a "stop-and-go" mode to reduce potential damage due to sample irradiation. The survey and detailed high resolution spectra (pass energy 25 and 10 eV, step size 1 and 0.1 eV, respectively) were recorded at room temperature using a Phoibos150-MCD energy analyzer. Powdered samples were deposited on a sample holder using double sided adhesive tape and subsequently evacuated under vacuum (<10–6 Torr) overnight. Eventually, the sample holder containing the degassed sample was transferred to the analysis chamber for XPS studies.

Magnetic properties of nanoparticles were measured by means of PAR 155 vibrating sample magnetometer (VSM) at room temperature from −10 to +10 kOe. The sample is rotated up to 360° w.r.t magnetic field and recorded in X-Y/(t) recorder.

The magnetic measurements were also performed on superconducting quantum interference device (SQUID)

Scheme 1 Ring opening polymerization of L-lactide

= Mn$_3$O$_4$ Nanoparticle
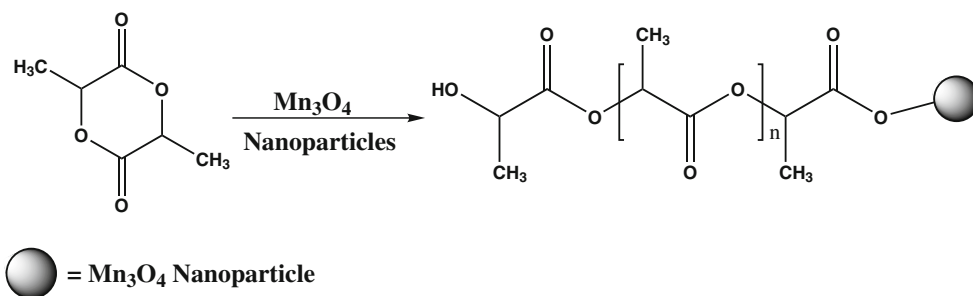
Fig. 1 TEM images of Mn$_3$O$_4$ nanoparticles
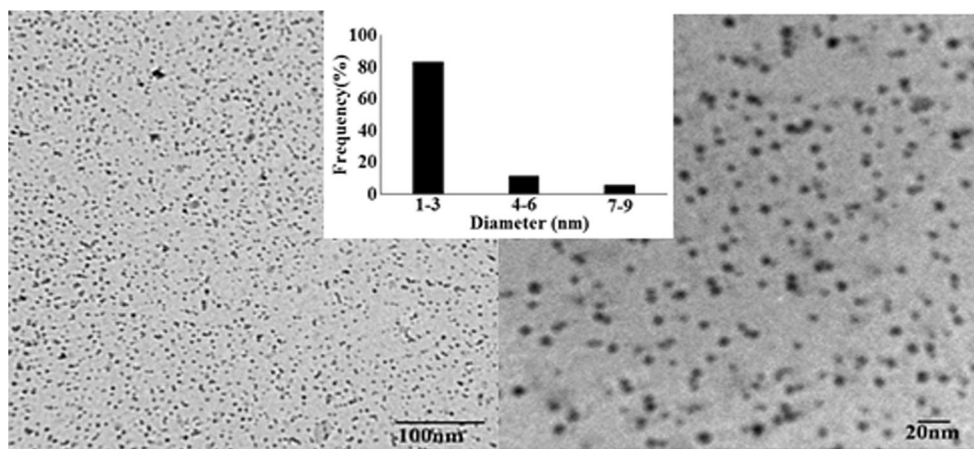
magnetometer (Quantum design MPMS XL-Evercool). The temperature ranged from 5 to 300 K in a zero-field cooling/field cooling (ZFC/FC) procedure at 100 Oe.

Results and discussion

The Mn$_3$O$_4$ nanoparticles were synthesized by microwave assisted solvo thermal process which involved trans-esterification of benzyl alcohol and manganese acetate. The synthesized nanoparticles were calcined at 500 °C. Bilecka et al. [27] have reported nanoparticles of various oxides from different precursors. However, prepared with slight modified procedure, our results showed that nanoparticles obtained from manganese acetate as precursor are that of Mn$_3$O$_4$. This was confirmed by XRD and the magnetic properties observed by VSM and SQUID.

Transmission electron microscopy is a useful tool to determine the size and shape of nanoparticles. TEM images of synthesized Mn$_3$O$_4$ nanoparticles are shown in the Fig. 1. The nanoparticles are almost spherical in shape and most of nanoparticles have size ranging from 1 to 3 nm. The blurriness of TEM images is due to magnetic nature of the Mn$_3$O$_4$ nanoparticles.

XRD of the calcined nanoparticle and non-calcined nanoparticle is shown in the Fig. 2. It can be seen that phase boundaries are not well defined in as prepared sample. However, after calcination these became clear and the diffraction pattern obtained was compared with the standard.

Obtained values confirm the formation of tetragonal phase of Mn$_3$O$_4$ in accordance with JCPDS 24–0735. The diffraction peaks were recorded and unit cell parameters were calculated (a = b = 5.761 Å, c = 9.46). These were comparable to the standard JCPDS values (a = b = 5.762 Å, c = 9.46 Å). The unit cell volume calculation (Table 1) of the particles is in agreement with the standard values [28].
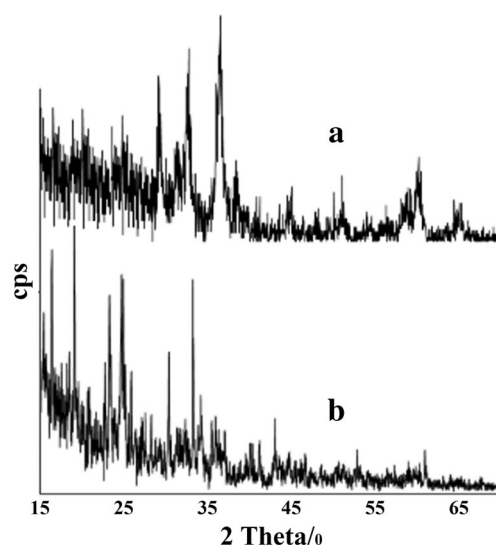

Fig. 2 XRD pattern of (**a**) Calcined and (**b**) Non calcined Mn$_3$O$_4$ Nanoparticles

Table 1 Calculated lattice parameters and unit cell volume

Observed d spacing	JCPDS values	(hkl)	Lattice parameter		Volume of unit cell Å	
			Calculated	Standard	Calculated	Standard
3.102	3.089	(112)	a = 5.761	a = 5.762	V = 313.9690	V = 314.407
2.776	2.768	(103)	b = 5.761	b = 5.762		
2.487	2.487	(202)	c = 9.46	c = 9.46		
2.039	2.0369	(220)				
1.795	1.798	(105)				
1.545	1.544	(224)				

Surface grafting of metal oxide nanoparticles is a useful tool to stabilize them and prevent their aggregation. It was carried out by ring opening polymerization of L-lactide. Many metal oxides have been reported as catalyst for the ring opening polymerization of L-lactide [29, 30]. To the best of our knowledge manganese oxide has not been tried as catalyst. With an aim to graft polymer onto the surface of nanoparticle we checked whether Mn_3O_4 can catalyze ring opening of L-lactide and got wonderful results. A series of polymerization reactions were carried out with concentration of metal oxide varying from 0.5 to 20% and polymerization confirmed by FTIR. Infrared spectrum of manganese oxide nanoparticles showed a few bands only due to stretching of metal oxide bonds, whereas those of nanocomposite showed a number of bands pertaining to the different groups present in the polymer chain. The results are depicted in Fig. 3. Only two main absorption bands observed at 520 and 633 cm^{-1} in the IR spectrum of Mn_3O_4 were attributed to the stretching modes of Mn-O. Presence of small broad absorption peaks between 3560 and 3500 cm^{-1} indicated the presence of surface hydroxyl groups. In the FTIR spectrum of Mn_3O_4/PLLA the most intense band at 1758 cm^{-1} was attributed to the ester group of PLLA main chain. The peaks at 1270, 1189 and 1132 cm^{-1} were attributed to -C-O stretching vibrations of ester in the main chain. The asymmetrical and symmetrical -CH_3 stretching of the methyl group in the side chains were observed at 2999 and 2881 cm^{-1}. The bending vibration of -CH_3 group was noticed at 1458 cm^{-1}. The stretching of -CH group present in the

Fig. 3 FT-IR of Mn_3O_4 nanoparticles, Mn_3O_4/PLLA nanocomposite (5% and 10%)
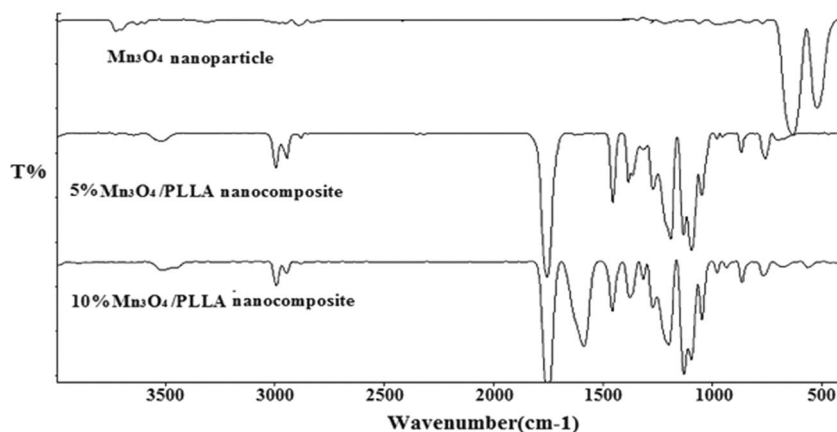
**Fig. 4** ^{1}H NMR and ^{13}C NMR of 2% Mn_3O_4/PLLA.

Fig. 5 TGA thermograms of Mn_3O_4/PLLA

Fig. 6 DSC thermograms of nanocomposites (0.5%, 2%, 5%)
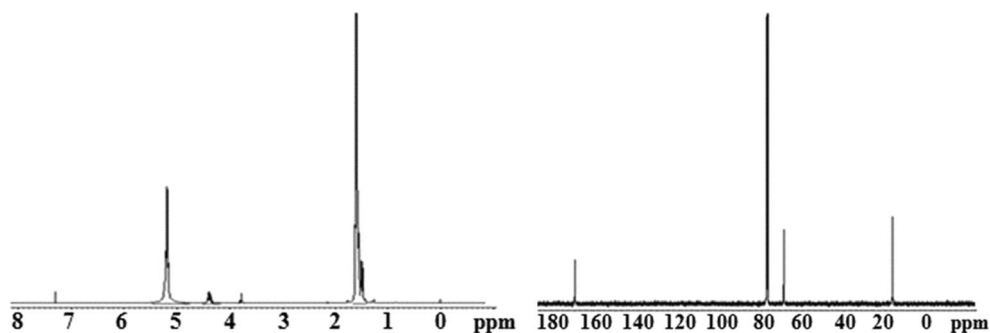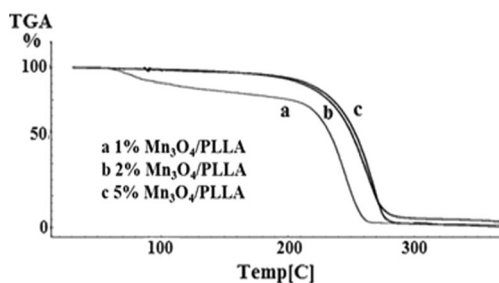
main chain of PLLA was observed at 2944 cm^{-1} and the corresponding bending vibration appeared between 1386 and 1362 cm^{-1}. A small peak observed at 1621–1604 cm^{-1} in the FT-IR spectrum of 5% nanocomposite was assigned to the O-C-O stretching of the chain ending carboxylate group through which the chain is attached to metal oxide surface. This peak increased in size with increase in metal oxide content in the Mn_3O_4/PLLA. Some workers observed that splitting of this band does not occur and in some cases proximity to the Mn_3O_4 nanoparticles may cause shift in the peak values.

NMR is another useful tool to confirm the formation of polymer chains. [1] H NMR spectra of different Mn_3O_4 /PLLA nanocomposites were taken but due to decreased solubility of the nanocomposite with increase in metal oxide content, no estimation of chain length was possible [See ESI]. ^{1}H NMR spectra of Mn_3O_4/PLLA are shown in the Fig. 4. The methine and methyl proton of the PLLA main chain were indentified due to peaks at 5.16 and 1.56 ppm respectively. The small peak at 3.75 ppm corresponds to hydroxyl end group. Another small peak at 4.36 ppm was assigned to the methine proton attached to terminal hydroxyl group. The optical purity of L-lactide was indicated by a quartet at 5.16 ppm. The peak at 7.82 ppm was due to CDCl$_3$. In the ^{13}C NMR (Fig. 5) of 2% Mn_3O_4/PLLA nanocomposite three major peaks were observed. The peak at 16.65 ppm was assigned to methyl group, 69.01 ppm to methine group and 169.62 ppm to carbonyl carbon. The triplet at 77.36 ppm is due to CDCl$_3$.

Thermal properties of synthesized nanocomposites were studied by TGA and DSC. Thermogravimetric analysis of nanocomposites was carried out to calculate the amount of polymer material incorporated into composite. TGA thermograms of Mn_3O_4/PLLA nanocomposites with different
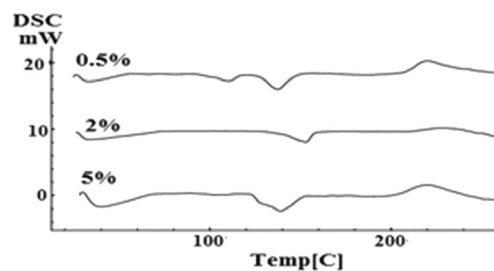
concentrations of Mn_3O_4 were carried out under nitrogen atmosphere and results are shown in Fig. 5. The weight loss (%) because of volatile products formed after decomposition was observed as a function of temperature. The degradation of polylactic acid chain occurs via unzipping mechanism. Initially degradation of nanocomposites was slow which was attributed to moisture present in it and unreacted monomers. In the end the degradation was fast because unzipping of polymer chain occured. The degradation patterns were found to be similar in (1%, 2% and 5%). Results summarized in Table 2 show decomposition temperatures for the composites are above 230 °C and the amount of residue left increases with the increase in the quantity of nanoparticles.

Differential scanning calorimetry is widely used to study thermal transitions. Glass transition temperature was not observed in any of the DSC thermograms (Fig. 6) and this was similar to our earlier observations with ZnO/PLLA nanocomposites [30]. Further the first small dip in the graph corresponds to the melting point of polymer and the data is given in Table 2. Melting point of various nanocomposites varied from 137 to 140 °C. This is considerably lower than that reported for pure PLLA. Also it was observed that at 0.5% of Mn_3O_4 probably two phases are present which melt at two different temperatures. These phase separation disappeared at higher loading of catalyst. At 5% loading a broad peak was observed and this point corresponded to the core/shell morphology observed by TEM. From both the TGA and DSC thermograms it was concluded that the decomposition of nanocomposite starts at around 220–260 °C.

The morphology of nanocomposites and size of nanoparticles was found from TEM images. At 2% loading it was observed that nanoparticles are uniformly dispersed in polymer matrix (Fig. SI). However, in the case of 5% Mn_3O_4/PLLA

Table 2 Summary of data derived from TGA and DSC curves

| Sr.No	Mn_3O_4/PLLA	Decomposition starts(°C)	Decomposition ends (°C)	Residue left at 300 °C (%)	Tm (°C)
1	0.5%	260	290	1.99	137.9
2	1%	230	260	2.78	139.1
3	2%	250	280	2.38	140.2
4	5%	250	290	5.68	139.3

core shell type morphology of nanocomposite was observed [31]. The size of spherical core shell particles varied between 70 to 180 nm. However, most of the particles were of less than 100 nm dimension. SEM image of 5% Mn$_3$O$_4$/PLLA (Fig. 7) taken from powdered sample showed small globules but they were tightly adhering to each other. EDAX analysis of 5% Mn$_3$O$_4$/PLLA showed 54.14% of carbon, 42.92% of oxygen and 2.94% of manganese (Fig. S3). As these values are area specific they may vary slightly from actual values.

XPS analysis gives the elemental composition of the surface atoms of nanocomposite. Figure 8 shows XPS analysis of 5% Mn$_3$O$_4$/PLLA nanocomposite. XPS analysis of Mn$_3$O$_4$/PLLA showed peaks corresponding to Mn 2p, C 1 s and O 1 s. The Mn 2p XPS spectra of composite exhibited two peaks at 642.9 and 641.0 eV corresponding to Mn 2p$_{1/2}$ and Mn 2p$_{3/2}$ spin orbital states of Mn$_3$O$_4$ respectively [32]. It was observed that there is energy separation of 11.9 eV between Mn2p $_{3/2}$ and Mn2p$_{1/2}$ peaks which is in accordance with the reported data of Mn 2p$_{1/2}$ and Mn 2p$_{3/2}$ in the spectrum of Mn$_3$O$_4$ [33]. There are four peaks of C1s for Mn$_3$O$_4$/PLLA in which are 284.94, 286.47, 289.76 eV were assigned to C-C, C- O and C = O respectively and the one at 288.80 eV to carboxylic group coordinating with Mn. Peaks observed in deconvoluted spectrum of O1s were 532.08, 532.36, 533.43 and 534.61 eV

which were assigned to Mn-O, C-O, C = O and H-O-H respectively [34].

Magnetization of nanoparticles and that of polymer coated nanoparticles was studied to check the effect of polymer coating on magnetic properties of the synthesized nanoparticles. Vibrating spin magnetometer (VSM) and Superconducting Quantum Interference Device (SQUID) were used to measure magnetic properties of both coated and uncoated nanoparticles. The magnetization curve of Mn$_3$O$_4$ nanoparticles at room temperature is shown in the Fig. 9a. The M-H curve is found to be linear with the fields and has zero coercivity at room temperature [35]. It has been reported that the hysteresis in the single-domain ferrimagnetic particles disappears, as particle size becomes small. This state of ferri-magnetism is called "superparamagnetism". In this case no hysteresis was found in M–H curve. Even when high magnetic field was applied the magnetization never became saturated. As the maximum anisotropy energy becomes close to the thermal energy at the room temperature, the process of flipping of the single-domain spin of nanoparticles becomes uninhibited [36] and magnetization curve shows no hysteresis which indicates the superparamagnetic character of the Mn$_3$O$_4$ nanoparticles [37, 38]. However, at a certain low temperature the situation may change and this was studied by SQUID analysis.

Fig. 7 (**a**) and (**b**) are TEM images of 5% Mn$_3$O$_4$/PLLA core shell nanocomposite (**c**) and (**d**) are SEM images 5% Mn$_3$O$_4$/PLLA nanocomposite.
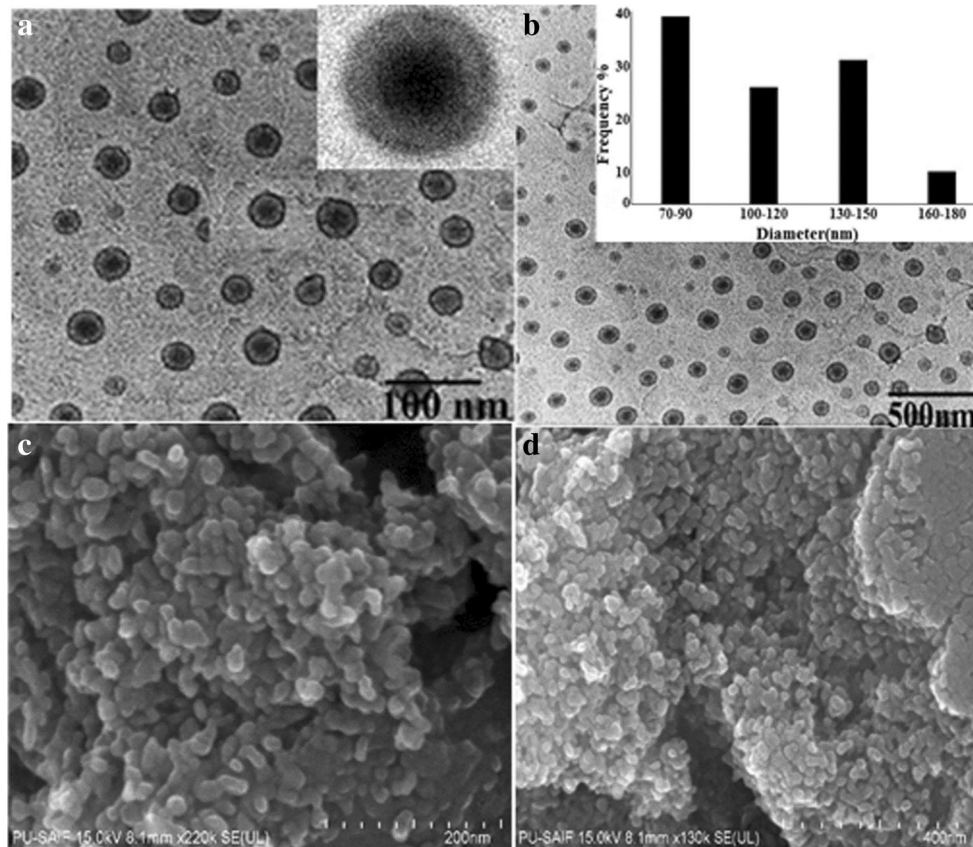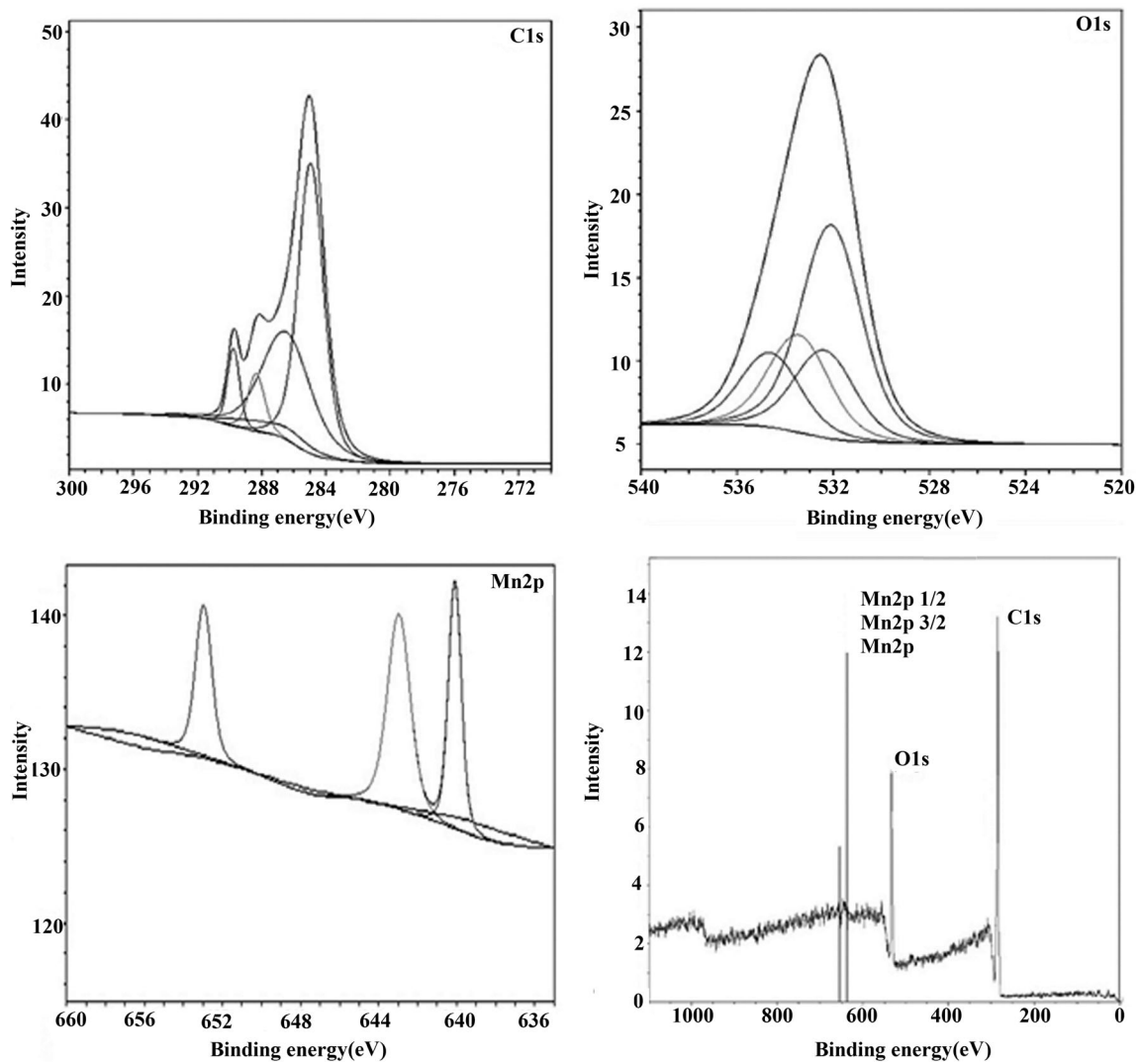
Fig. 8 XPS of 5% Mn_3O_4/PLLA

SQUID magnetometer was used to study the magnetic properties of nanoparticles at different temperature (Fig. 9b). The temperature dependence of magnetization of the sample was measured with the use of zero field cooling (ZFC) and field cooling (FC) procedures in the applied magnetic field of 100 Oe at temperature between 5 to 300 K. There was pronounced difference between the two curves and phenomenon of superparamagnetic blocking of magnetic nanoparticles was clearly observed. The uncoated particles are ferromagnetic and show some ferromagnetic interaction between each other. The temperature where the two curves split is known as the blocking temperature and it was observed at 40 K. Above this temperature the particles are still ferromagnetically ordered, but the magnetization of each particle is pointing in a random

Fig. 9 Hysteresis loop and plot of magnetization vs temperature of Mn_3O_4 NPs at 100 Oe
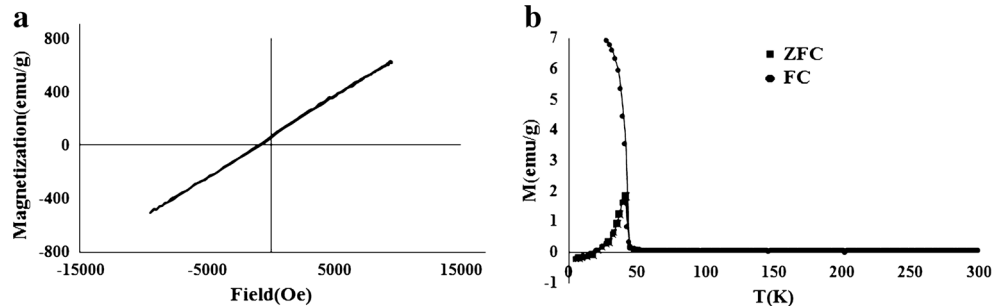
Fig. 10 Magnetization curve under applied magnetic field of (a) 5% Mn_3O_4/PLLA nanocomposites (b) 20% Mn_3O_4/PLLA nanocomposites
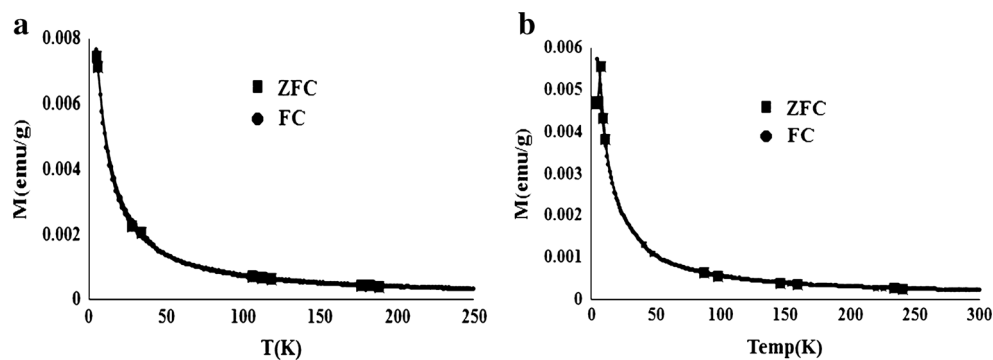
direction. Essentially the system behaves like a paramagnet and such a paramagnet is called a superparamagnet as the individual moments are not those of the individual atoms but those of the individual particles. Below this blocking temperature, the magnetization of a particle is no longer free to rotate on the time scale of the experiment but is frozen in a certain orientation. This freezing of the orientation is dictated by the applied field and the interaction between particles. Hence, the pronounced difference between ZFC and FC. Literature available on the magnetic behaviour of Mn_3O_4 nanoparticles also supports this observation [39–41].

To study magnetization of the nanocomposite, two different concentrations were prepared i. e. 5% Mn_3O_4 / PLLA and 20% Mn_3O_4 / PLLA. The temperature dependence of magnetization on 5% and 20% Mn_3O_4 /PLLA is shown in Fig. 10. The FC magnetization curve was an exact duplicate of the ZFC pattern in both the cases, which demonstrates that only one magnetic phase exists [42, 43]. There is no pronounced blocking temperature anymore. The loss of splitting between ZFC and FC can be due to many reasons. It may be due to stress caused by different expansion rates of nanoparticles and polymer or it may be due to large paramagnetic contribution of individual nanoparticles [44] In addition it may also be that the interaction between the particles is completely suppressed after polymer coating. Further, studies to understand this behavior is in progress.

Conclusion

We have successfully synthesized Mn_3O_4 nanoparticles of size 1–3 nm by microwave enhanced process. We were also able to coat synthesized Mn_3O_4 nanoparticles by PLLA resulting in core shell structures in a facile single step. It was concluded that Mn_3O_4 nanoparticles can catalyse ring opening polymerization of L-lactide and result in surface grafting. VSM and SQUID studies of nanoparticles showed that individual Mn_3O_4 nanoparticles were ferromagnetic but behaved as superparamagnetic above blocking temperature of 40 K. However, after surface grafting no noticeable blocking

temperature was observed either due to stress caused by surface grafting or complete loss of interactions between individual particles. Further work is in progress to understand the magnetic behavior of Mn_3O_4/PLLA nanocomposites.

References

1. Hussein AK (2015) Applications of nanotechnology in renewable energies—a comprehensive overview and understanding. Renew Sust Energ Rev 42:460–476
2. Fan Z, Huang X, Tan C, Zhang H (2015) Thin metal nanostructures: synthesis, properties and applications. Chem Sci 6:95–111
3. Bogunia-Kubik K, Sugisaka M (2002) From molecular biology to nanotechnology and nanomedicine. Biosystems 65:123–138
4. Patsula V, Moskvin M, Dutz S, Horák D (2016) Size-dependent magnetic properties of iron oxide nanoparticles. J Phys Chem Solids 88:24–30
5. Pankhurst QA, Connolly J, Jones SK, Dobson J (2003) Applications of magnetic nanoparticles in biomedicine. J Phys D Appl Phys 36:167–181
6. Perez JM, Josephson L, O'Loughlin T, Hogemann D, Weissleder R (2002) Magnetic relaxation switches capable of sensing molecular interactions. Nat Biotechnol 20:816–820
7. Sun C, Lee JSH, Zhang MQ (2008) Magnetic nanoparticles in MR imaging and drug delivery. Adv Drug Deliv Rev 60:1252–1256
8. Fattahi H, Laurent S, Liu F, Arsalani N, Elst LV, Muller RN (2011) Magnetoliposomes as multimodal contrast agents for molecular imaging and cancer nanotheragnostics. Nanomedicine 6:529–544
9. Shin TH, Choi Y, Kim S, Cheon J (2015) Recent advances in magnetic nanoparticle-based multi-modal imaging. Chem Soc Rev 44:4501–4516
10. Mody VV, Cox A, Shah S, Singh A, Bevins W, Parihar H (2014) Magnetic nanoparticle drug delivery systems for targeting tumor. Appl Nanosci 4:385–392
11. Unsoy G, Khodadust G, Yalcin S, Mutlu P, Gunduz U (2014) Synthesis of Doxorubicin loaded magnetic chitosan nanoparticles for pH responsive targeted drug delivery. Eur J Pharm Sci 62:243–250

12. Bhatnagar SP, Rosensweig RE (1995) Introduction to the magnetic fluids bibliography. J Magn Magn Mater 149:198

13. Solanki A, Kim JD, Lee KB (2008) Nanotechnology for regenerative medicine: nanomaterials for stem cell imaging. Nanomedicine 3:567–578

14. Serantes D, Simeonidis K, Angelakeris M, Chubykalo-Fesenko O, Marciello M, Morales MP, Baldomir D, Martinez-Boubeta C (2014) Multiplying Magnetic Hyperthermia Response by Nanoparticle Assembling. J Phys Chem C 118:5927–5934

15. Dutz S, Hergt R (2014) Magnetic particle hyperthermia—a promising tumour therapy? Nanotechnology 25:452001

16. Audran RGL, Huguenard AP (1981) Magnetic recording elements containing transparent recording layer. US Patent 4,302,523

17. Ziole RF, Webster NY (1984) Developer composition containing superparamagnetic polymers. US Patent 4,474,866

18. McMichael RD, Shull RD, Swartzendruber LJ, Bennett LH, Watson RE (1992) Magnetocaloric effect in super paramagnets. J Magn Magn Mater 111:29–33

19. Shafi KVPM, Ulman A, Dyal A, Yan X, Yang N, Estournès C, Fournès L, Wattiaux A, White H, Rafailovich M (2002) Magnetic Enhancement of γ-Fe_2O_3 Nanoparticles by Sonochemical Coating. Chem Mater 14:1778–1787

20. Lai J, Shafi KVPM, Ulman A, Yang N, Cui M, Vogt T, Estournès C (2003) Mixed iron-manganese oxide nanoparticles. Prepr Pap-am Chem Soc Div Fuel Chem 48:729–730

21. Seo WS, Jo HH, Lee K, Kim B, Oh SJ, Park JT (2004) Size-dependent magnetic properties of colloidal Mn_3O_4 and MnO nanoparticles. Angew Chem Int Ed 43:1115–1117

22. Djerdj I, Arčon D, Jagličic Z, Niederberger M (2007) Nonaqueous Synthesis of Manganese Oxide Nanoparticles, Structural Characterization, and Magnetic Properties. J Phys Chem C 111:3614–3623

23. Laurent S, Forge D, Port M, Roch A, Robic C, Vander Elst L, Muller RN (2008) Magnetic iron oxide nanoparticles: Synthesis, Stabilization, Vectorization, Physicochemical characterization and biological applications. Chem Rev 108:2064–2110

24. Pugazhvadivu KS, Ramachandran K, Tamilarasan K (2013) Synthesis and Characterization of Cobalt doped Manganese Oxide Nanoparticles by Chemical Route. Physics Procedia 49:205–216

25. Bose VC, Biju V (2015) Optical, electrical and magnetic properties of nanostructured Mn_3O_4 synthesized through a facile chemical route. Physica E 66:24–31

26. Raquez J-M, Habibi Y, Mararu M, Dubois P (2013) Polylactide (PLA)-based nanocomposites. Prog Polym Sci 38:1504–1542

27. Bilecka I, Elser P, Niederberger M (2009) Kinetic and Thermodynamic Aspects in the Microwave-Assisted Synthesis of ZnO Nanoparticles in Benzyl Alcohol. ACS Nano 3:467–477

28. Raj AME, Victoria SG, Jothy VB, Ravidhas C, Wollschlager J, Suendorf M, Neumann M, Jayachandran M, Sanjeeviraja C (2010) XRD and XPS characterization of mixed valence Mn_3O_4 hausmannite thin films prepared by chemical spray pyrolysis technique. App Surf Sci 256:2920–2926

29. Kricheldor HR, Serra A (1985) Polylactones 6: Influence of various metal salts on optical purity of poly (L-Lactide). Polym Bull 14:497–502

30. Kaur H, Rathore A, Raju S (2014) A study on ZnO nanoparticles catalyzed ring opening polymerization of L-lactide. J Polym Res 21:537–547

31. Si PZ, Li D, Choi CJ, Li YB, Geng DY, Zhang ZD (2007) Large coercivity and small exchange bias in Mn_3O_4/MnO nanoparticles. Solid State Commun 142:723–726

32. Wang D, Li Y, Wang Q, Wang T (2012) Facile Synthesis of Porous Mn_3O_4 Nanocrystal–Graphene Nanocomposites for Electrochemical Supercapacitors. Eur J Inorg Chem 2012:628–635

33. An GM, Yu P, Xiao MJ, Liu ZM, Miao ZJ, Ding KL, Mao LQ (2008) Low-temperature synthesis of Mn_3O_4 nanoparticles loaded on multi-walled carbon nanotubes and their application in electrochemical capacitors. Nanotechnology 19:275709

34. Luo Y, Wang X, Xu D, Wang Y (2009) Preparation and characterization of poly (lactic acid)-grafted TiO2 nanoparticles with improved dispersions. App Surf Sci 255:6795–6801

35. Rohani Bastami T, Entezari MH (2012) A novel approach for synthesis of superpramagnetic Mn_3O_4 nanocrystals by ultrasonicbath. Ultrason Sonochem 19:560–569

36. Ozkaya T, Baykal A, Kavas H, Koseoglu Y, Toprak MS (2008) A novel synthetic route to Mn_3O_4 nanoparticles and their magnetic evaluation. Phys B 403:3760–3764

37. Du J, Gao Y, Chai L, Zou G, Li Y, Qian Y (2006) Hausmnnite Mn_3O_4 nanorods: synthesis, characterization and magnetic properties. Nanotechnology 17:4923–4928

38. Sicard L, Le Meins J-M, Methivier C, Herbst F, Ammar S (2010) Polyol synthesis and magnetic study of Mn_3O_4 nanocrystals of tunable size. J Magn Magn Mater 322:2634–2640

39. Borovik-Romanov AS, Orlova MP (1957) Magnetic properties of manganese oxides at temperatures from 20 to 300 K. J Exp Theor Phys 32:1255

40. Dwight K, Menyuk N (1960) Magnetic properties of Mn_3O_4 and canted spin problem. N Phys Rev 119:1470–1479

41. Lei S, Tang K, Fang Z, Zheng H (2006) Ultrasonic-Assisted Synthesis of Colloidal Mn_3O_4 Nanoparticles at Normal Temperature and Pressure. Cryst Growth Des 6:1757–1760

42. Kang C, Cai H, Zhang X, Tang J, Xu P, Li M, Zong H (2015) The study of high Curie temperature ferromagnetism properties in Mn-doped SiC thin film. Results Phys 5:178–181

43. Martinez B, Obradors X, Balcells L, Rouanet A, Monty C (1998) Low Temperature Surface Spin-Glass Transition in γ-Fe_2O_3 Nanoparticles. Phys Rev Lett 80:181–184

44. Inamdar DY, Lad AD, Pathak AK, Dubenko I, Ali N, Mahamuni S (2010) Ferromagnetism in ZnO Nanocrystals: Doping and Surface Chemistry. J Phys Chem C 114:1451–1459